Behavior of Meandering Overbank Channels with Graded Sand Beds

P. R. Wormleaton[1]; R. D. Hey, M.ASCE[2]; R. H. J. Sellin, M.ASCE[3]; T. Bryant[4]; J. Loveless[5]; and S. E. Catmur[6]

Abstract: Measurements of velocity distributions, depth variation, and sediment transport have been made under bankfull and overbank flow conditions in meandering channels with a graded sand bed, using the large-scale U.K. Flood Channel Facility. The overbank conditions depend upon the relative strength of opposing secondary circulation cells generated by shear at the channel crossover and centrifugal forces around the meander bend. Generally the shear-generated secondary flow either reversed or weakened the centrifugal circulation around the next downstream bend. This led to considerable modification of the main channel bed morphology, which, in turn, altered flow distributions. Measurements of the lateral distribution of bed load were made using a $\frac{1}{4}$-scale Helley–Smith sampler. This demonstrated that the bed load was generally concentrated within a limited width of the channel and tended to take the shortest route through the meanders. Comparisons of observed and calculated bed material load gives an indication of how secondary circulation around meanders, under both bankfull and overbank conditions, affects the predictive performance of formulas derived for predominantly one-dimensional flow.

DOI: 10.1061/(ASCE)0733-9429(2005)131:8(665)

CE Database subject headings: River flow; Flow patterns; Flood plains; Meandering streams; Channel morphology; Sediment transport.

Introduction and Background

Global climate change has already led to many rivers, throughout the World, flooding more often and for longer periods of time than before. Consequently, it is becoming increasingly important, for economic, environmental, and public safety reasons, to understand the behavior of rivers in flood. This understanding feeds into the design of flood alleviation works, floodplain management strategies, and accurate prediction of flood events.

The lowland reaches of rivers, which are generally the most highly populated, are often characterized by meanders. The bed morphology of these rivers is determined by the local geology, the characteristics of material transported from upstream, the discharge, and local flow distribution. The relationship between river morphology and flow distribution is mutually dependent, with changes in one affecting the other. In particular a change in the morphology can alter the depth of flow for a particular discharge, and hence the extent of any flooding.

Bankfull flow in a meandering channel is characterized by centrifugal circulation generated around the bends, which dies out and reverses direction alternately between bends. However, if the channel flows out of bank into a predominantly straight floodplain, as shown in Figs. 1(a and b), there will be interference between the main channel and floodplain flows, particularly in the region of the crossover points. This interference will create a secondary circulation in the main channel, which will reinforce the centrifugal circulation created around the upstream meander bend. However, as the flow proceeds into the next bend, the centrifugal circulation will change polarity. Thus the two circulation cells will tend to counteract each other. The flow patterns in a meandering channel with overbank flow are thus largely determined by the relative strength of these secondary cells, generated by channel/floodplain interaction at the crossover and centrifugal forces around the apex. If the floodplain velocities are relatively high, typically with smooth floodplains and/or higher depths, then the circulation at the crossover may be strong enough to be carried well into or through the downstream apex as observed by Sellin et al. (1993) and shown in Fig. 1(a). On the other hand with lower floodplain velocities the centrifugal circulation will predominate through the apex as shown in Fig. 1(b). Large scale laboratory experiments with rigid boundary overbank meandering channels (Sellin et al. 1993; Shiono and Muto 1998; Loveless et al. 1999, 2000; O'Sullivan 1999) have shown how this interaction

[1]Senior Lecturer, Dept. of Engineering, Queen Mary, Univ. of London, Mile End Rd., London E1 4NS, U.K. E-mail: p.r.wormleaton@qmul.ac.uk

[2]Professor, School of Environmental Sciences, Univ. of East Anglia, Norwich NR4 7TJ, U.K. E-mail: r.hey@uea.ac.uk

[3]Emeritus Professor, Dept. of Civil Engineering, Univ. of Bristol, Queens Bldg., University Walk, Bristol BS8 1TR, U.K. E-mail: r.h.j.sellin@bristol.ac.uk

[4]Accountant, PricewaterhouseCoopers, 31, Great George St., Bristol, BS1 5QD, U.K. E-mail: tom.bryant@uk.pwcglobal.com

[5]Senior Lecturer, Dept. of Civil Engineering, Univ. of Bristol, Queens Bldg., University Walk, Bristol BS8 1TR, U.K. E-mail: j.loveless@bristol.ac.uk

[6]Senior Lecturer, Dept. of Civil Engineering, Univ. of East London, Barking Campus, Longbridge Rd., London RM8 2AS, U.K. E-mail: s.e.catmur@uel.ac.uk

Note. Discussion open until January 1, 2006. Separate discussions must be submitted for individual papers. To extend the closing date by one month, a written request must be filed with the ASCE Managing Editor. The manuscript for this paper was submitted for review and possible publication on March 26, 2003; approved on November 22, 2004. This paper is part of the ***Journal of Hydraulic Engineering***, Vol. 131, No. 8, August 1, 2005. ©ASCE, ISSN 0733-9429/2005/8-665–681/ $25.00.

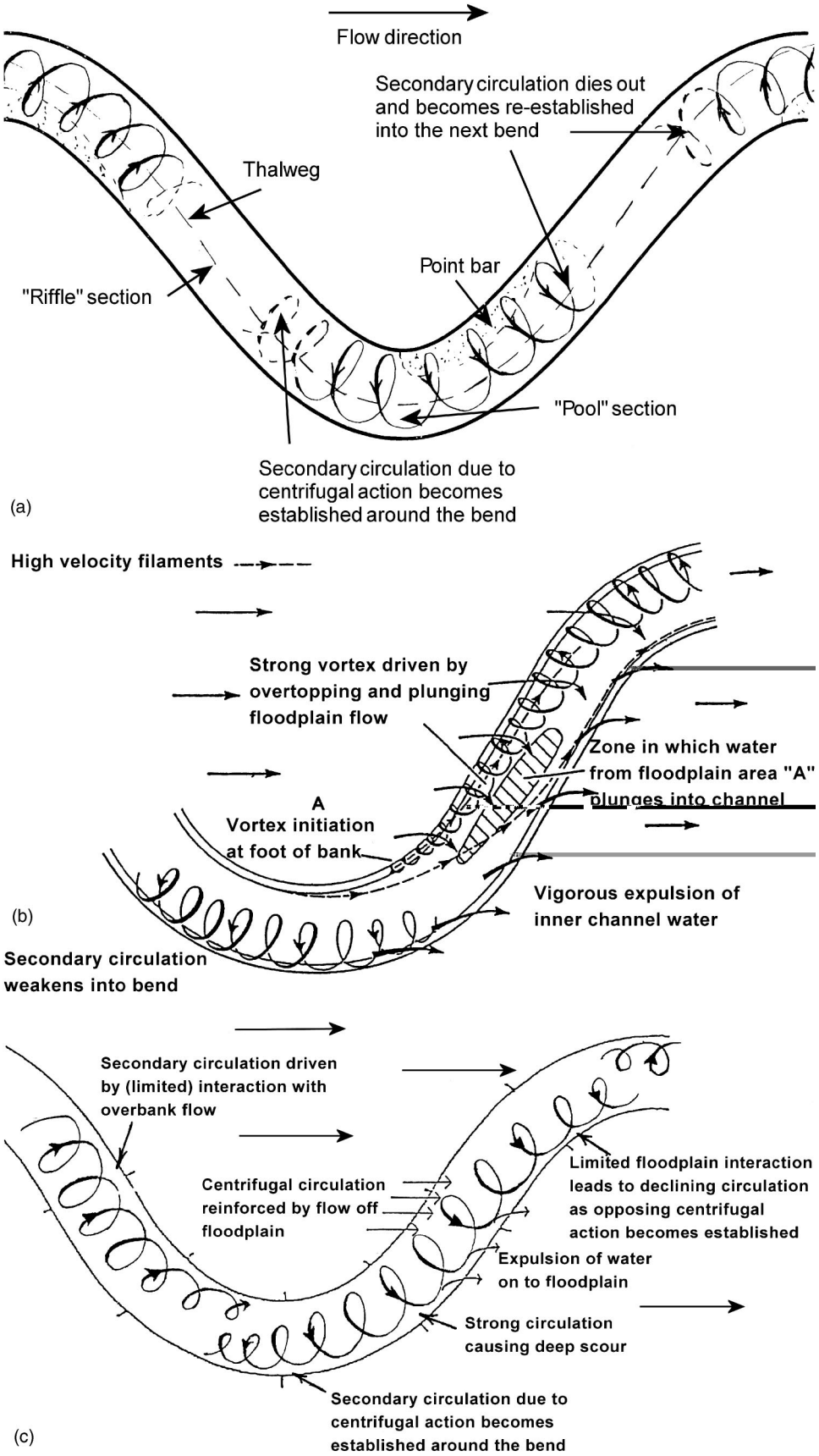

Fig. 1. Flow structures in meandering channels with floodplains: (a) in-bank, (b) overbank with smooth floodplain (after Sellin et al.), (c) overbank with rough floodplain

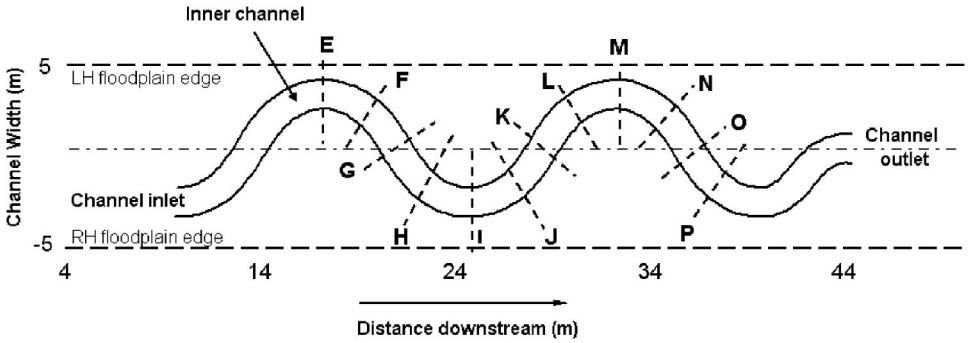

Fig. 2. Layout of meandering channel in the U.K. Flood Channel Facility showing location of measuring sections

between floodplain and channel flows profoundly affects primary velocities, secondary circulation, and boundary shear stress distributions within the main channel. They also highlight the potential impact of this interaction on flood levels and conveyance.

Experiments have been reported on meandering channels with mobile beds consisting of single-size sediment (O'Sullivan 1999; Myers et al. 2000). These were carried out under equilibrium conditions in uniform flow. Valuable data were obtained of bed profiles and also the response of sediment transport rates to overbank flow. In this paper the effect of graded bed material on flow and sediment transport processes with both bankfull and overbank flows are reported. As natural river sediments are graded, this can promote behavior, such as sorting and armoring, that does not occur with uniform material. These processes can significantly modify the hydraulic and morphological characteristics of the channel.

To summarize therefore; flow in meandering rivers is characterized by relatively strong secondary circulation due to centrifugal forces around each bend, which, in part, determines the bed morphology. However, when a meandering stream spills over onto the adjacent floodplain, interaction between the predominantly down valley floodplain flow and the meandering river channel significantly modifies flow distribution and secondary circulation. This in turn leads to changes in the morphology, which may well modify flood levels. It will also affect the sediment transport capacity of the river channel, with the possible consequences of downstream erosion or deposition.

Clearly, if these processes are to be correctly accounted for in river management and numerical modeling schemes, then a sound understanding of the underlying physics is essential. This paper sets out to address these issues.

Experiments on the U.K. Flood Channel Facility

The experiments described in this paper were carried out on the U.K. Flood Channel Facility (FCF) at HR Wallingford. The FCF consists of a 10-m-wide and 60-m-long tank, within which main channel and associated floodplain layouts can be constructed. Flow is introduced at the upstream end to a maximum discharge of 1 m^3/s. Sediment can be recirculated and fed into the test channel through a reciprocating feeder in order to maintain an even lateral distribution. At the downstream end the sediment is trapped in a large tank from where it can be sampled and recirculated. The sediment feed and trap arrangements limited the usable test length in the FCF for these experiments to 35 m as shown in Fig. 2. A view of the FCF, looking upstream, is seen in Fig. 3, and it is described more fully by Knight and Sellin (1987).

A series of experiments were undertaken on the FCF to investigate the relation between flow and sediment transport processes in a meandering channel with a graded mobile bed. A sine generated meandering channel with a sinuosity of 1.34, crossover angle of 60°, and wavelength of 14.96 m was used in all tests. This was formed with concrete sides and a sand/gravel bed. The main channel had a top width of 1,600 mm with 45° side slopes, and the bed was initially screeded horizontally to a depth of 150 mm below floodplain level. In order to correspond to a natural river with cohesive or composite banks, the main channel outer bank was gradually increased to vertical around the apices. The floodplain had a valley slope of 0.00183 with no lateral variation in level. The channel layout is given in Fig. 2, which also shows the cross-section notation.

The grading of the bed material was chosen in order to avoid the general formation of ripples since, as these do not scale, their size would have dominated flow and transport processes. The material was only partially mobile under overbank test flows, thereby enabling sorting processes to occur. The material had a $d_{16}=0.35$ mm, $d_{50}=1.33$ mm, and $d_{84}=3.19$ mm. The sediment

Fig. 3. Photograph of the U.K. Flood Channel Facility showing the roughening strips

Table 1. Principal Parameters of the Flood Channel Facility Tests Analyzed in this Paper

Experiment reference	Floodplain roughness	Floodplain form	Discharge (m^3/s)	Depth over floodplain (mm)	Depth ratio
Bankfull					
BF	—	—	0.097	−6.4	0.957
Overbank					
HOSW	Smooth	Wide straight	0.449	68.9	1.315
LORW	Rough	Wide straight	0.120	42.5	1.221
HORW	Rough	Wide straight	0.164	75.7	1.335

Note: BF=bankfull flow; HOSW=high overbank flow with smooth floodplain; LORW=low overbank flow with rough floodplain; and HORW=high overbank flow with rough floodplain.

was recirculated and introduced evenly across the width of the main channel by use of a moving arm mechanism.

In the tests reported herein, the floodplain was straight, 10-m wide with no lateral slope and longitudinal slope of 1.83×10^{-3}. Tests were carried out with a smooth concrete floodplain and also with an artificially roughened floodplain. The roughening on the floodplain consisted of a series of perforated metal strips laid across the floodplain perpendicular to the valley slope. These are discussed more fully by Sellin et al. (2003). The layout of the perforated strips can be seen in Fig. 3.

The test series reported herein comprised a bankfull flow (BF), low and high overbank flows with a roughened wide floodplain (LORW and HORW, respectively), and high overbank flow with a smooth wide floodplain (HOSW). An outline of the test parameters is given in Table 1. In this table the depth ratio is defined as flow depth above average main channel bed/bankfull average depth.

Prior to all tests the main channel was screeded to a uniform depth of 150 mm below the floodplain level with well-mixed bed material. The discharge was then set at around bankfull and run until equilibrium conditions were achieved in the main channel (no further change in bed levels or systematic changes in recirculated sediment load were observed). For overbank flow tests, the discharge was then increased to the required level and again run to equilibrium. This sequence was adopted in order to model flooding conditions in a real river. Thus the channel morphology was allowed to develop first under bankfull conditions before the flood was applied.

Measurements of discharge, three-dimensional point velocities, equilibrium depth profiles, bed load magnitude and grading distribution, and bed material grading distribution were taken at selected sections around the test meander bends. The measurement of discharge and velocity have been discussed elsewhere by Loveless et al. (1999, 2000) and Wormleaton et al. (2004).

The lateral distribution of bed load in the main channel was obtained using a $\frac{1}{4}$-scale Helley–Smith sampler. Measurements were taken over a period of 5 min at transverse intervals of 100 mm. The total *integrated bed load* for the section could be found by summing these individual readings. In addition to this, measurements of *total sediment load* were taken by sampling from the sediment recirculation system. These measurements were taken at intervals of 5 min continuously for a period of between 5 and 6 h (i.e., 60–72 samples).

Flow Characteristics

The characteristics of the primary and secondary velocity distributions observed in these experiments have been described in earlier papers (Loveless et al. 1999, 2000; Wormleaton et al. 2004). However, since the distribution of the sediment transport is intimately coupled to the flow characteristics, it is as well to briefly review the latter as a prelude to consideration of the former.

Bankfull Flow Test Bankfull Flow

The observed bed profiles at bankfull in Fig. 4 exhibited point bar morphology with riffles at the crossovers. This is typical of many rivers as identified by Dietrich (1987) and reproduced here in Fig. 5. The thalweg follows the outer bank of the bend until it moves across the riffle just downstream of the crossover toward the outside of the following bend.

The bankfull velocity distributions in Fig. 4 show a large centrifugal secondary cell around the meander bend, which maintains the transverse slope of the bed from the deep outer bank to the point bar on the inner bank. This circulation cell continues downstream of the apex and through the following crossover. It then dissipates as a counterrotating circulation is established in the next bend. The bar and bed forms developed are shown in the bed mosaic in Fig. 6. The fast flowing sections are picked out by the large grains exposed on the bed. These trace a path from the inner bank at the entrance to the bend to the outer bank downstream of the apex, which corresponds to that seen by Dietrich (1987) in Fig. 5. The avalanche fronts of the low bed sheets are at right-angles to the near-bed flow direction and indicate that they move from the inner to the outer bank just upstream of the bend. Slower flow in the lee of the point bar in the vicinity of the crossover is indicated by smaller exposed bed material creating ripple formations. Around the bend apex the exposed grain sizes vary from large in the deeper section at the outer bank to small on the bar at the inner bank. This sorting is due to the centrifugal secondary circulation, which drives smaller particles further up the transverse slope toward the inner point bar than the larger ones. Such behavior has been observed and modeled by a number of researchers, e.g., Dietrich et al. (1979), Julien (1997), Parker and Andrews (1985).

Overbank Flows with Straight Floodplain

Smooth Floodplain (Test High Overbank Flow with Smooth Floodplain)

Equilibrium channel bed profiles and velocity distributions during overbank flow with the smooth straight floodplains at a depth ratio (=flow depth above average channel bed level/bankfull average depth) of 1.315 are shown in Fig. 7. It is clear that overbank flow significantly modifies the flow structure and bed profile in the main channel from that at bankfull. The key to this adjustment appears to be the strength of the circulation imposed upon the main channel flow by the floodplain flow in the region of the crossover. Here the high velocity flow on the floodplain jets into the slower in-channel flow at an obtuse angle, whereby generating a horizontal interface at bankfull level. This view is upheld by Shiono and Muto (1998). Their observations of Reynolds' stresses in a rectangular rigid bed meandering channel indicated that shear

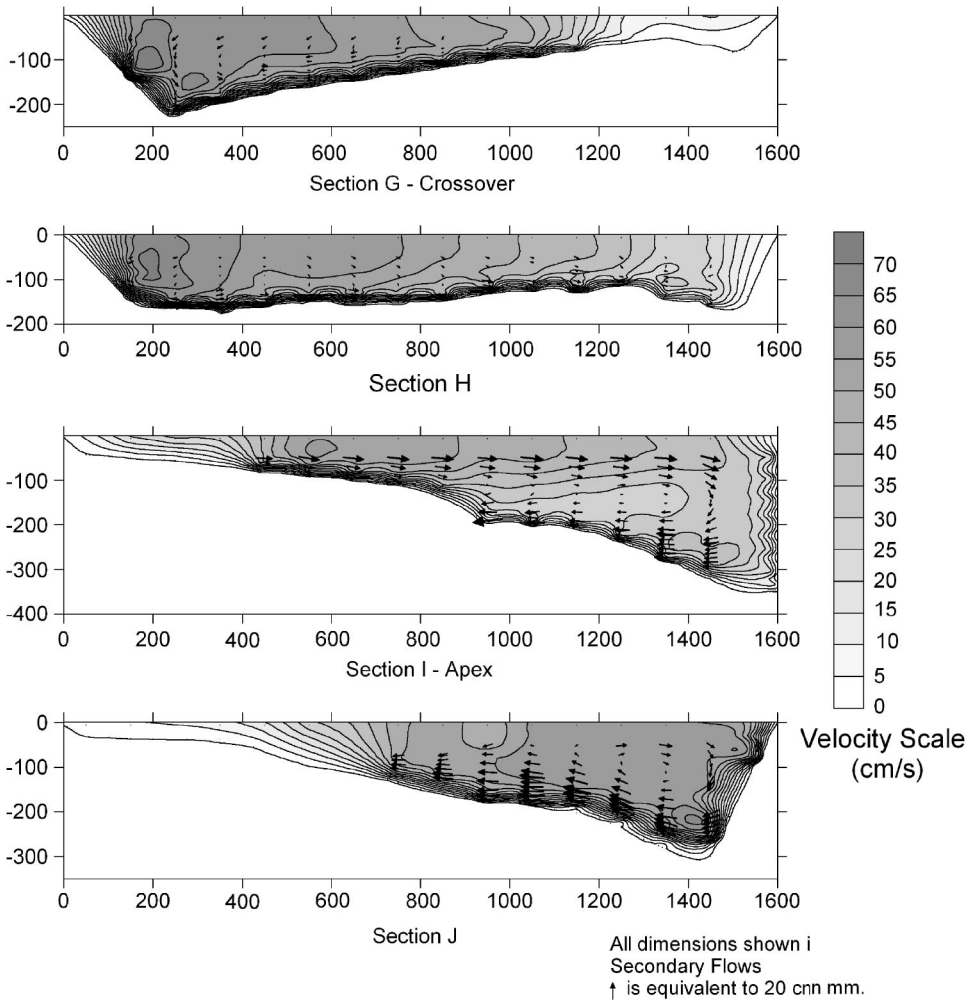

Fig. 4. Primary and secondary flow patterns for bankfull flow

generated turbulence in the region of the horizontal interface at bankfull level can be more influential than bed generated turbulence.

In Fig. 7 the floodplain flow induces a counterclockwise circulation at crossover G looking downstream. This circulation is sufficiently robust to counteract the opposing centrifugal circulation at the next downstream bend I, and so it continues through the apex. This leads to an overall interactive mechanism similar to that observed by Sellin et al. (1993) for rigid bed meandering channels with relatively smooth floodplains, which is shown in Fig. 1(a). The evidence for this is seen in the bed profile at the apex, which shows deposition on the outer bank and erosion near to the inner bank. This is the reverse of the bankfull flow case and indicates a reversal in the secondary flow direction. It is also noticeable that the erosion at the outer bank just downstream of the apex is less in this high overbank case than for the bankfull flow. This is simply because the reversed circulation at the apex opposes rather than complements the circulation due to floodplain interaction in this region.

Roughened Floodplain (Tests Low Overbank Flow with Roughened Wide Floodplain and High Overbank Flow with Roughened Wide Floodplain)

The results of the overbank tests with roughened floodplains are quite different from those with the smooth floodplain. This underscores the importance of the balance between channel/floodplain interaction in the region of the crossover and centrifugal forces around the apex in the channel forming process. The Manning n for the rough floodplains was 0.105 and 0.120, respectively, for the low (LORW) and high (HORW) overbank flows, which is an order of magnitude greater than the value of 0.011 for the isolated smooth floodplains. Therefore the channel/floodplain interaction in the region of the crossover is considerably reduced from that in the smooth floodplain case and the flow mechanism resembles that shown in Fig. 1(b).

The bed profiles and general circulation patterns for the rough overbank flows, at depth ratios of 1.221 and 1.335, are shown in Figs. 8 and 9. A secondary circulation is imposed upon the bankfull flow at the channel crossover point in a similar manner to the

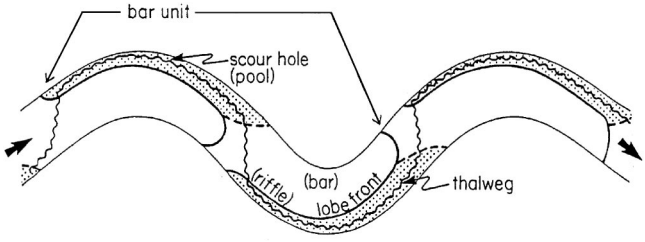

Fig. 5. Meandering channel bed morphology (after Dietrich)

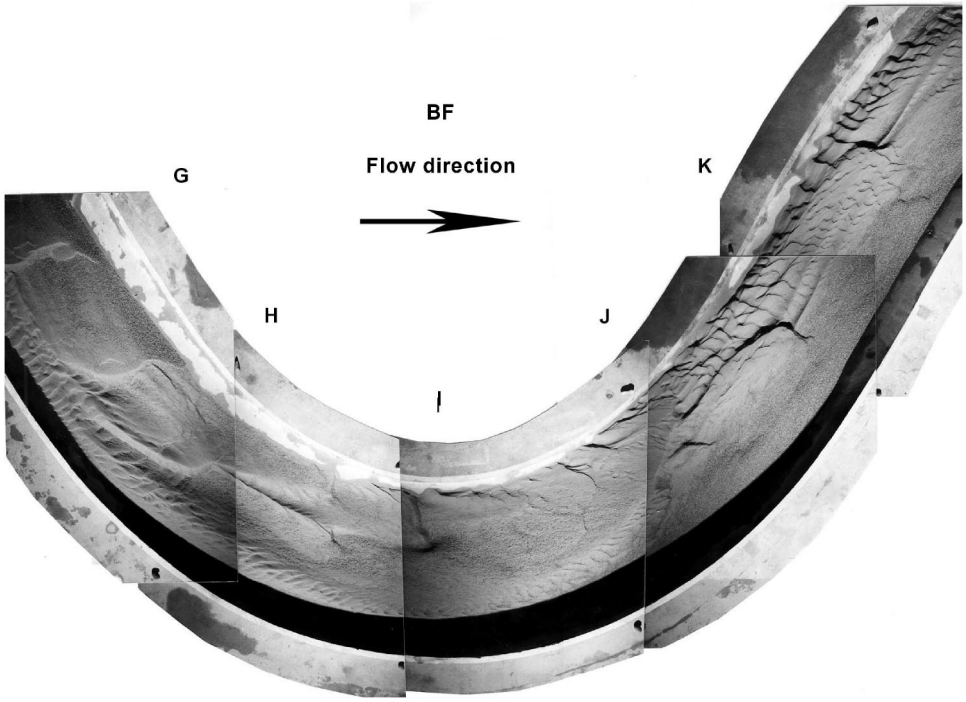

Fig. 6. Aerial photograph mosaic of bed morphology for bankfull flow (BF)

smooth floodplain case. However, this circulation cell is not sufficiently robust to overcome the counterrotating centrifugal cell at the next apex as was the case for the high smooth floodplain flow, although it may persist toward the apex on the inside bank. Consequently a centrifugal secondary cell has established itself at the outside of the bend apex. At the lower depth ratio of 1.221 the main channel/floodplain interaction at the crossover G is very weak and so the counterrotating (clockwise) centrifugal cell is able to become well established at the outer bank of the downstream bend I. The relatively steep face of the bed profile at the apex clearly indicates strong circulation here. There is a flattening of the bed around the inner bank at the bend apex, which is due to the canceling out of the opposing circulation cells in this region. The net result is a shoaling of the channel bed extending to the outer portion of the channel away from the bank. As the depth ratio increases to 1.335 the channel/floodplain interaction at the upstream crossover becomes stronger. This enables the resulting circulation cell to continue through the inside of the apex eroding the inner point bar. A weak centrifugal cell forms around the outside of the apex, causing a slight rise in the bed near the outer bank at the apex where the two opposing circulations meet. Just downstream of the apex at section J, the centrifugal circulation cell becomes very well developed, due to it being reinforced by the floodplain flow. Dye tracing experiments described by Loveless et al. (2000), show a strong ejection of water from the main channel onto the floodplain here. Clearly, this is an area where bank erosion is most likely to occur. Shoaling at the inner bank is noticeable in this region fed by the strong circulation at the outer bank. The vertical photograph mosaic in Fig. 10 shows the high velocity thalweg on the downstream (left) bank at the crossover G. Velocities on the right side are much lower with the result that the bed material is finer and the surface is rippled. Between sections H and the apex I, the thalweg moves toward the outside of the channel. It is noticeable that, in contrast to bankfull flow, the bed material is of similar size across the whole of the bed around the apex. This is because the sorting mechanism induced by the strong centrifugal circulation at bankfull no longer exists with the consequence that the bed has relatively uniform depth. By section J the thalweg has moved to the outer (right) bank, causing considerable local erosion, while the strong secondary circulation leads to considerable deposition of smaller bed material with ripple bed forms near the inner bank.

Summary

When flow in a meandering channel is at, or below, bankfull, the major source of secondary flow is centrifugal circulation generated around the bend apex. This is carried downstream into the crossover before it dissipates on entering the next bend. The circulation creates and maintains the point bar on the inner bank. With graded bed material, the smaller size fractions are driven further toward the inner bank around the apex producing a transverse variation in bed material size.

Overbank flow introduces a second major source of secondary circulation, due to interaction between the channel and floodplain flows in the region of the crossover (G). This reinforces the centrifugal circulation from the upstream apex and opposes that at the downstream apex. General flow structure in meandering channels with overbank flows is dictated by the relative strengths of these two major sources of circulation. If the interaction circulation is sufficiently strong then it may persist into the next apex reducing the effect of the centrifugal circulation and eroding the inner point bar in this region. However, downstream of the apex the interaction and centrifugal circulations combine to produce a strong secondary flow, which erodes the outer bank and maintains an inner point bar. The net effect of floodplain interaction is thus to shift the location of the point bar on the inner bank downstream of the apex. As overbank flow levels increase, the riffle, pool, and point bar features were displaced progressively further downstream.

Although natural flood events will rarely be sustained long enough for the river to adjust to the new flow condition, nevertheless the experiments do indicate that the locations of pools and

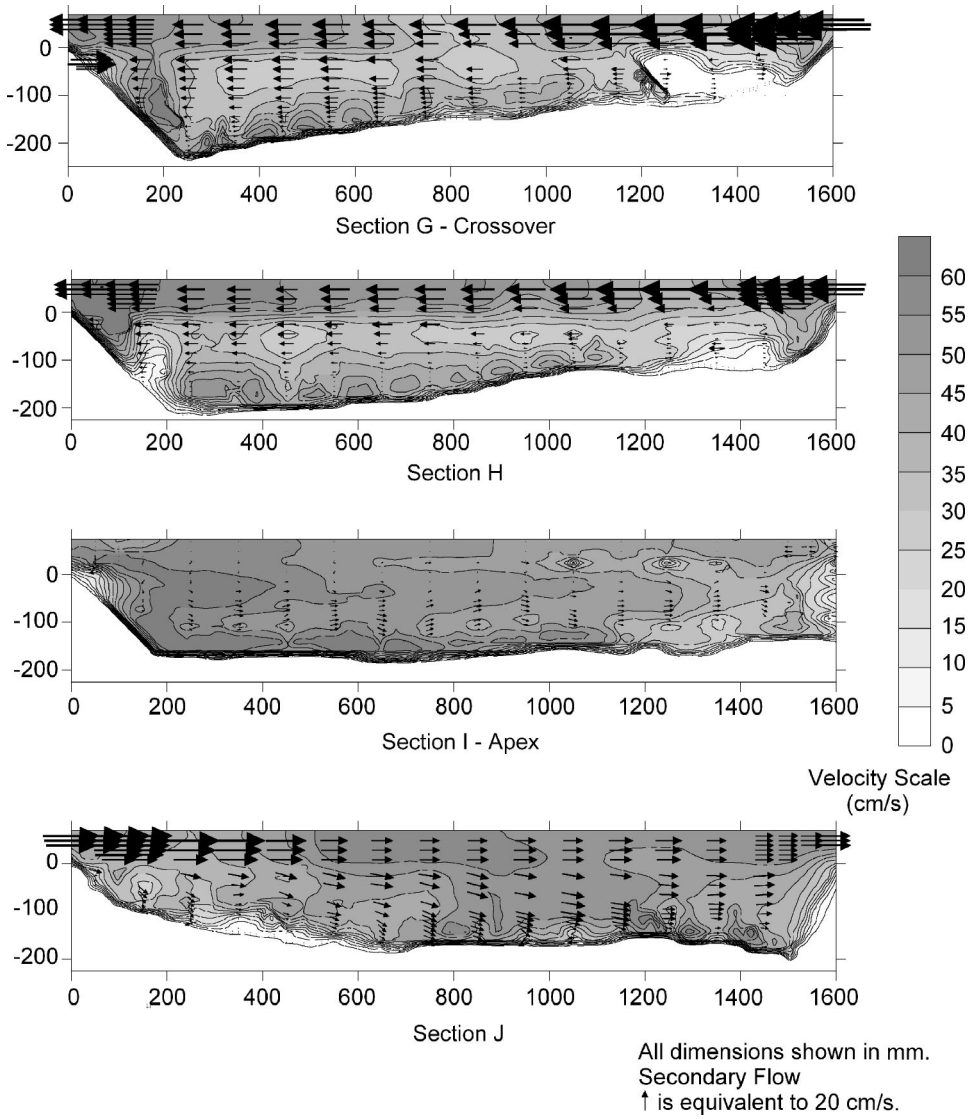

Fig. 7. Primary and secondary flow patterns for high overbank flow with smooth floodplain

riffles could be affected during a flood. Should increased bank shear stresses cause bank failure, then the changes would become permanent. Significantly, as the highest stresses occur downstream from the meander apex, it will encourage downstream meander migration.

Morphology and Sediment Transport

Variation in Cross-sectional Area

Each experimental run commenced with a well-mixed horizontal bed in the main channel, initially screeded horizontal to a depth of 150 mm below floodplain level. This was run to equilibrium at bankfull flow. Figure 11 shows the changes in cross-sectional area around the test meander during this initial bankfull phase. The classic riffle/pool sequence with a significant deposition of bed material, or decrease in cross-sectional area, at the crossover and erosion around the apex are clearly seen in this figure.

Overbank flow was then applied, and Figs. 12 and 13 show the consequent changes in the equilibrium main channel cross-sectional areas, through the meander, from those at bankfull. In the case of the smooth floodplain (HOSW), overbank flow results in bed erosion downstream of the crossover, which occurs on the down-valley side of the channel (section H in Fig. 13). This is due to the large secondary circulation caused by the intense main channel/floodplain interference around the crossover. Due to this secondary flow, some of the material eroded is transferred locally to the up-valley side of the channel, thus reducing the net local erosion. This circulation (which is in the opposite sense to the bankfull centrifugal circulation) continues, albeit with reduced magnitude, into the apex. Consequently, the point bar, established in the initial bankfull flow phase, is eroded from the inside of the bend. At the same time, the initial outer bank erosion, caused by the strong centrifugal secondary circulation at bankfull flow, is filled, resulting in a general lateral leveling of the bed and overall local deposition. This general leveling out of the bed by removal of the point bar and filling at the outside of the bend continues for a short distance downstream of the apex (section J), before encountering erosion on entering the next crossover region.

With the roughened floodplain (HORW), there is considerable local erosion between the crossover and the apex. The interference between the main channel and floodplain is less severe than

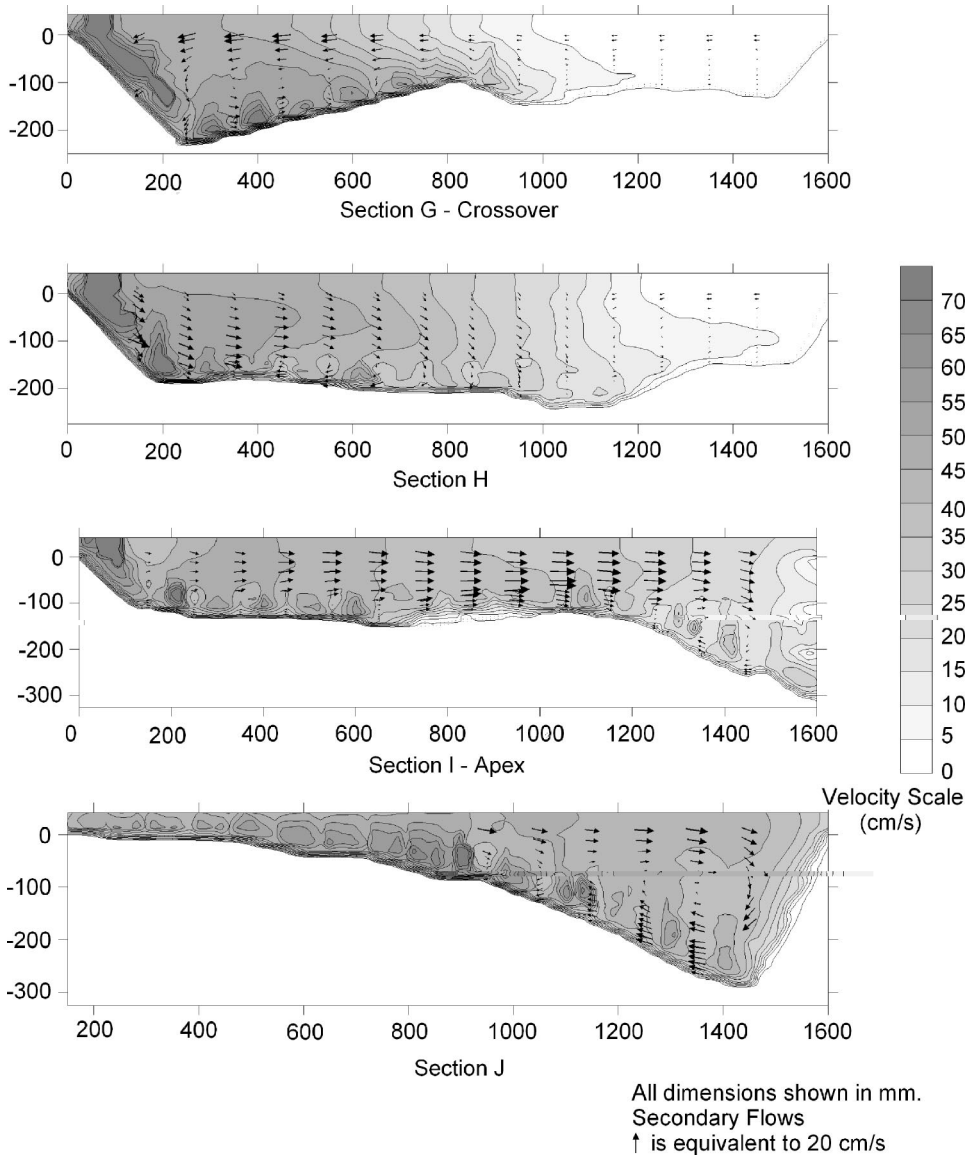

Fig. 8. Primary and secondary flow patterns for low overbank flow with rough floodplain

for the smooth floodplain case, although it still leads to erosion near the down-valley bank. However, the weaker interference allows centrifugal circulation to establish itself more readily near the outer channel bank, thereby reducing the degree of bed material deposition in this region relative to that for the smoother floodplain (section H). The overall result is considerable erosion in this part of the channel as seen in Fig. 12. A similar situation continues through to the apex, with removal of the inner point bar, but restricted filling on the outside of the bend due to the onset of centrifugal circulation (section I). Downstream of the apex, secondary circulation becomes stronger as the floodplain interference reinforces the centrifugal circulation. The bed level near the outer bank is very similar to the bankfull case, possibly due to bed armoring preventing any further erosion in this region where the larger grains are exposed. However, the strong circulation supports a steep lateral profile locally, and the eroded material from upstream of the apex is deposited here as a greatly enhanced inner point bar (section J).

The variation in cross-sectional area for the lower overbank flow (LORW) is not shown in Fig. 12 or Fig. 13, in order to retain clarity when comparing the other two flows. However, as might be expected, it follows the general high overbank (HORW) variation, being smaller in magnitude but very similar in distribution through the meander.

In summary, both the smooth and rough floodplains caused main channel erosion in the approach to the bend due to the interaction circulation. In the case of the smooth floodplain, this circulation is carried strongly into the apex and leads to erosion of the inner point bar and deposition at the outer bank. This outer bank deposition is eroded downstream of the apex causing a general leveling of the cross-section at this point. The interactive circulation is relatively less intense for the roughened floodplain and is counteracted by centrifugal circulation at the apex. The resultant circulation is not strong enough to support the inner point bar, or to create the outer bank deposition that occurred with the smooth floodplain. Thus there is overall erosion around the apex. The material eroded from the apex and upstream is then deposited as a large bar on the inner bank just downstream of the apex (at J). It is noticeable (see Fig. 7) that the larger interaction circulation generated by the smooth floodplain leads to less overall erosion or deposition at cross-sections around the meander than the smaller interaction produced by the rough floodplain. The

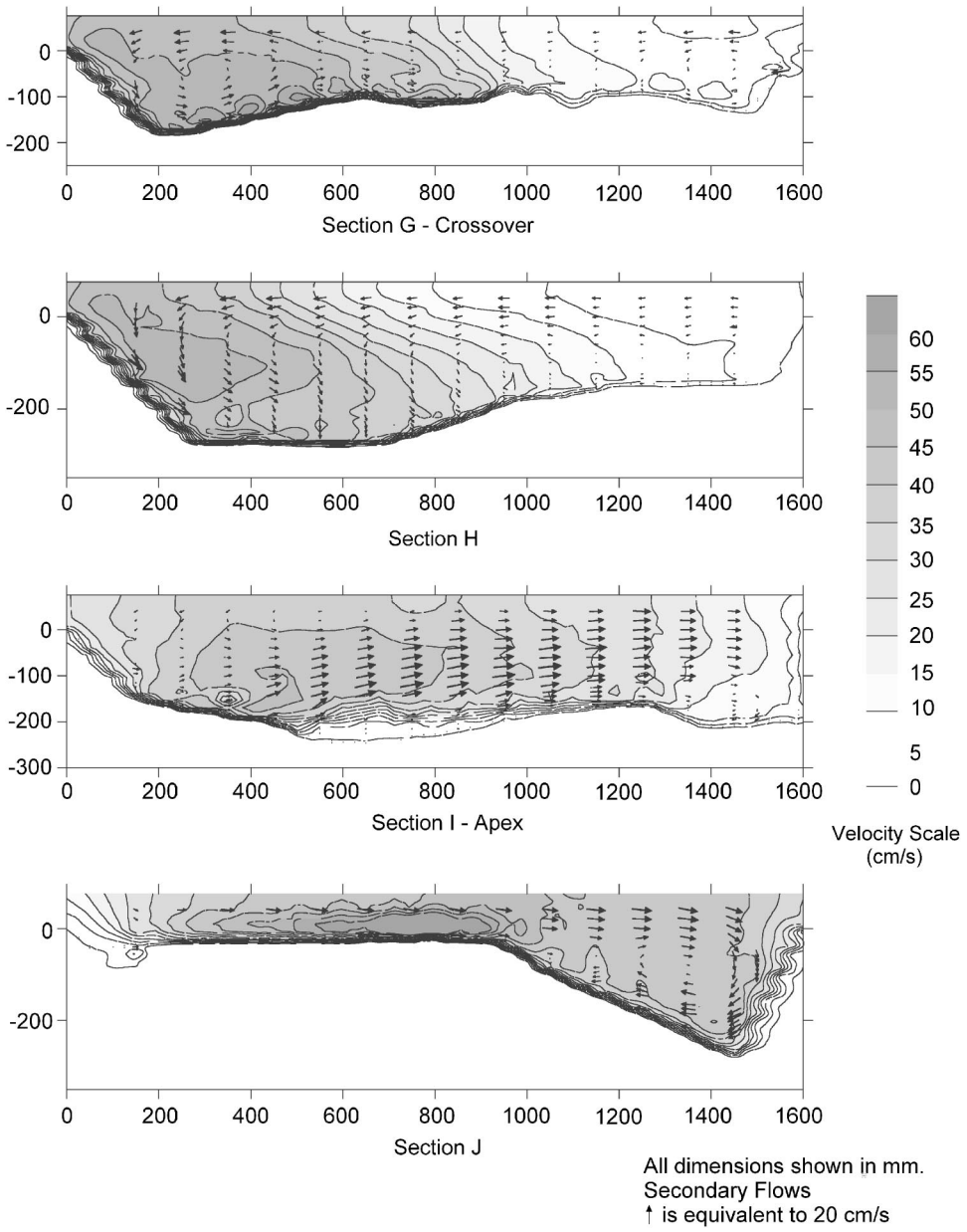

Fig. 9. Primary and secondary flow patterns for high overbank flow with rough floodplain

key to this difference is the deposition of material around the outside of the apex for the smooth floodplain, which reduces net local erosion and provides less material for formation of the large downstream inner bar that was created by the rough floodplain.

Overall Sediment Transport

The *total sediment load* was measured by taking samples of 5 min duration continuously over a period of 5–6 h. These samples were taken from the reciprocating feeder arm, weighed wet, and then replaced. The water content was found over a large number of samples to be reasonably constant with 90% confidence limits of 18.0±1.4%, enabling the samples to be corrected to dry weight.

Variations in the relative sediment transport rate (total/bankfull sediment transport rate) with depth ratio for the bankfull and overbank flows are shown in Fig. 14. Comparative results are given in the same figure for similar planform meandering chan-

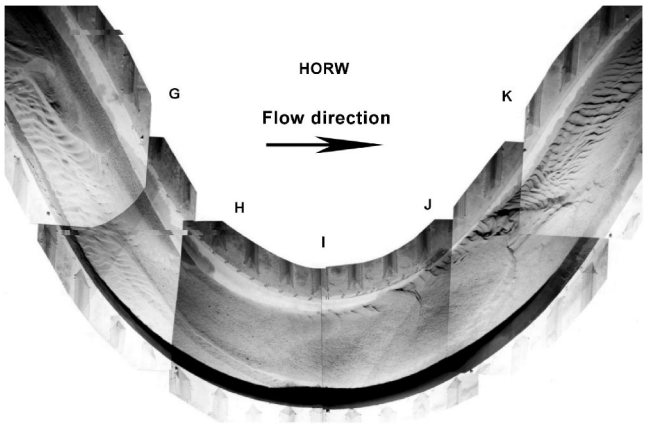

Fig. 10. Aerial photograph mosaic of bed morphology for high overbank flow with rough floodplain

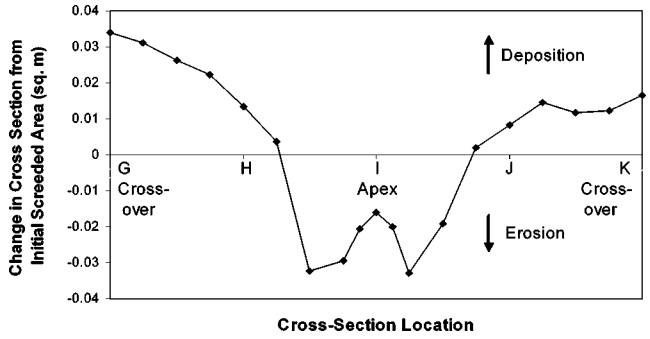

Fig. 11. Changes in main channel cross-sectional area around a meander between initially screeded cross-sections and bankfull equilibrium cross-sections

nels having a uniform sand bed with d_{50} of around 0.85 mm. These are taken from O'Sullivan et al. (1999) and Rameshwaran et al. (1999). O'Sullivan et al. obtained their results from the FCF, whilst Rameshwaran et al. used a $\frac{1}{4}$ scale model of the FCF. Each set of results displays a similar trend with a reduction of sediment transport from bankfull up to a depth ratio in the range 1.15–1.25, and then an increasing sediment transport rate as the floodplain depth rises further.

This decrease in sediment transport at low overbank depths can only be due to main channel/ floodplain interaction, which would generally act to reduce the main channel velocities and hence boundary shear stresses below those at bankfull. The changes in main channel mean velocity below floodplain level between bankfull and overbank flows, as a percentage of the bankfull mean velocity, are plotted in Fig. 15 for one meander length. Clearly for the case of the roughened floodplain there is a general decrease in velocity at both low and high overbank depths, which is most marked at the crossovers. The high overbank smooth floodplain flow shows a general decrease in main channel velocity except at the apex. The increase in velocity at the apex is because the floodplain and main channel flows are aligned and, in this particular case, the mean floodplain velocity is 6% greater than the main channel velocity. The increase in velocity at this point and decrease at all other points around the meander suggests that a proportion of the sediment transport is carried by the floodplain flow.

The results show that as the flow goes overbank the sediment transport falls significantly from its bankfull value, and it does not

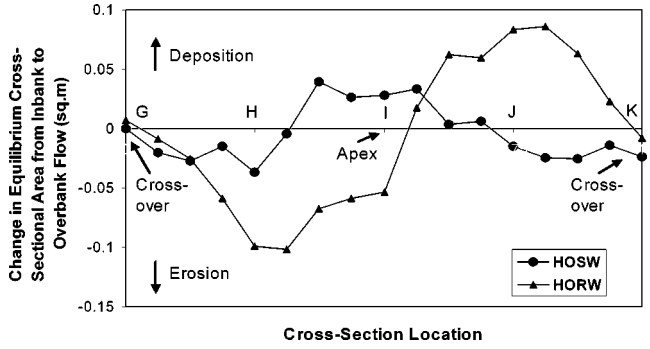

Fig. 12. Changes in main channel cross-sectional area around a meander between bankfull and overbank equilibrium cross-sections with smooth (high overbank smooth wide) and rough (high overbank rough wide) floodplains

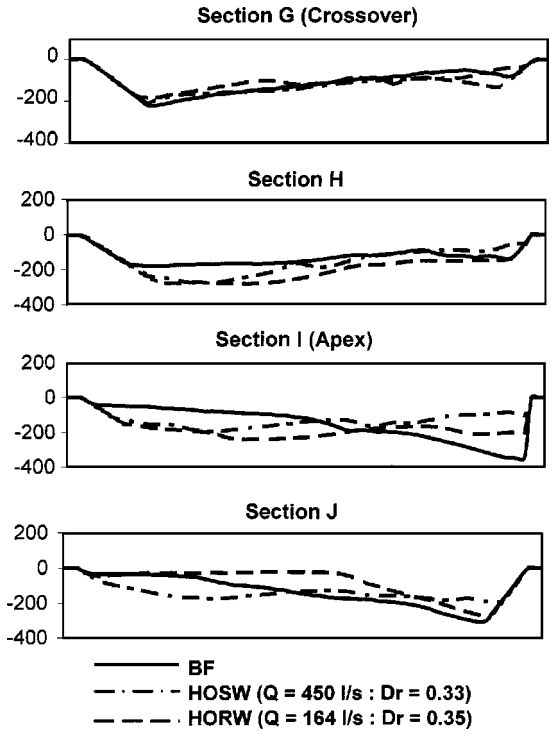

Fig. 13. Comparison of main channel bed profiles between bankfull (BF), and overbank flows with smooth (high overbank smooth wide) and rough (high overbank rough wide) floodplains

return to that value until the flow is 3–4 times bankfull discharge. This lends credence to the concept that bankfull flow is the dominant channel forming discharge as it, in the longer term, transports most sediment (Wolman and Miller 1960). It also reinforces the use of bankfull as a practical flow upon which to base channel morphological design, as recommended by Hey (1978).

Lateral Distribution of Bed Load

The lateral distribution of bed load in the main channel was sampled using a 1/4-scale Helley–Smith sampler (19 mm orifice) attached to a supporting rod. This was similar to that devised by Dietrich and Smith (1984) for sampling bed load transport of fine sand and granules that were being mobilized over migrating bed forms. The size of the orifice meant that it effectively avoided sampling any material transported in suspension. Care was exer-

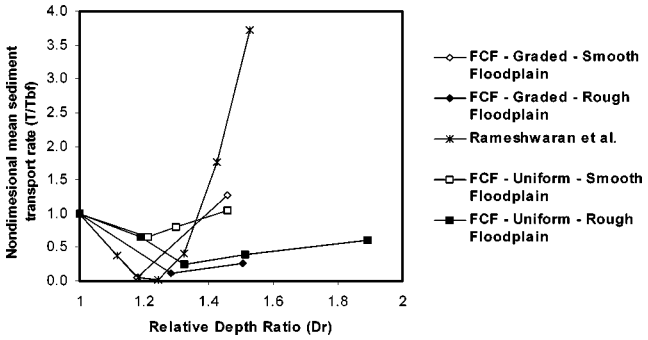

Fig. 14. Variation of main channel total sediment load ratio (overbank sediment load/bankfull sediment load) with relative depth ratio (floodplain depth/main channel depth)

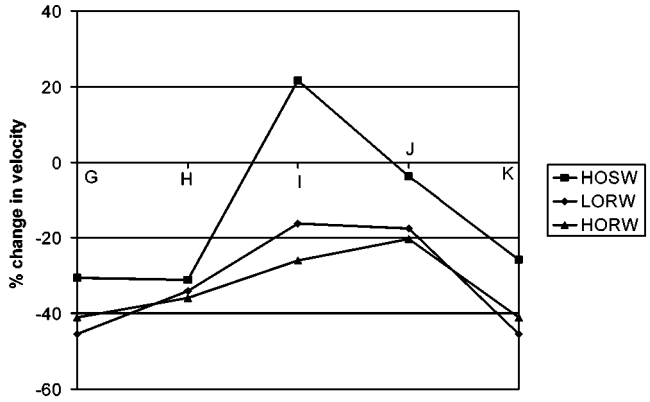

Fig. 15. Variation of percentage change in main channel average velocity (below floodplain level) for overbank flows, relative to bankfull value, through a meander

cised to support the sampler on the bed to prevent bed scour at the lip and, hence, an overestimation of the transport rate. With regard to the alignment of the sampler, this ideally needs to be parallel to the trajectory of the transported bed material (Dietrich and Smith 1984). Due to the clarity of the flow, it was possible to observe the trajectory of the transported material, and whether the sampler caused any convergence on, or divergence from, the orifice, thus affecting the sediment-trapping efficiency of the sampler. In these experiments it was observed that, since the movement of the bed material was generally near parallel to the banks of the main channel, aligning the sampler perpendicular to the main channel cross-section caused little or no convergence or divergence near its orifice. Bed load readings were taken at sections K ,L, M, N, and O as shown on Fig. 2.

Each dune migrating through the test bend adjusted its footprint and height in response to variations in shear stress patterns around the meander bend. This consistency, and the fact that there was no systematic change in bed levels at each measured cross-section over time, indicates that the sampled bed load integrates the bed load transport manifest as dune migration plus any additional throughput load. As bed load transport rates will vary between maximum at the dune crest and minimum at the dune trough, care was exercised to ensure that the bed load sampling was undertaken over a period, depending upon the dune passage, sufficient to determine the temporal mean bed load.

The bed load readings from the Helley–Smith sampler at 100 mm lateral increments across the section allowed for the distribution of the bed load to be studied. The total bed load could also be obtained by summing the individual bed load readings across the section. This is referred to as the *integrated bed load*. It should be distinguished from the measured *total sediment load*, which is obtained from readings in the recirculation system as described earlier.

Comparisons between the integrated bed load and measured total sediment load readings are given in Fig. 16. The total sediment load readings showed some scatter, although the time series were generally stationary indicating equilibrium conditions. The movement of bed forms through the system would contribute toward the spread of the data, but no regular cyclic pattern could be readily discerned from the time series. Samples of 5 min duration are probably too long to capture such data reliably. The mean values and 90% confidence limits for these total sediment load readings are shown in Fig. 16, which gives an indication of the degree of pulsing even under stable conditions.

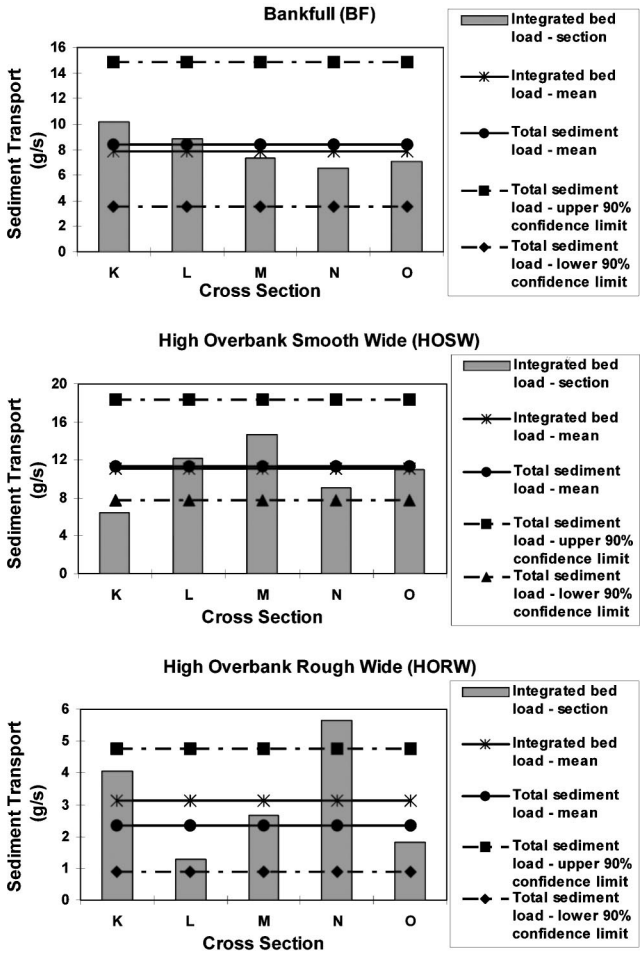

Fig. 16. Comparison of *integrated bed load* (from the Helley–Smith sampler) and *total sediment load* (from the downstream settlement tank) readings for bankfull (BF) and high overbank flows (high overbank smooth wide and high overbank rough wide)

Also shown in Fig. 16 are the integrated bed load transport rates for individual cross-sections and the mean of these through a meander. In the two relatively high sediment transport cases, i.e., BF and HOSW, the agreement between the mean values for total sediment and bed load are very close indeed. This implies only small amounts of suspended load or low errors. There is some variation in the integrated bed loads between cross-sections. This should not occur in equilibrium conditions. However, the movement of bed forms through the section would affect these results. It should be borne in mind that a cross-section needs 16 lateral readings with the Helley–Smith sampler, each lasting 5 min, requiring a total of some 2.5 h allowing for resetting the sampler. Moreover in the high overbank smooth floodplain case (HOSW), it was suggested earlier that some of the sediment transport might be carried over the floodplain. The integrated bed load readings corroborate this, with a high sediment transport value at the apex and lower values around the rest of the meander. This would suggest an expulsion of sediment onto the floodplain from the main channel outer bank downstream of the bend, which would be reintroduced into the main channel upstream of the equivalent bend one wavelength downstream.

The high overbank roughened floodplain (HORW) case shows greater variation than the other two between the mean total and bed loads and also between the individual cross-sectional bed

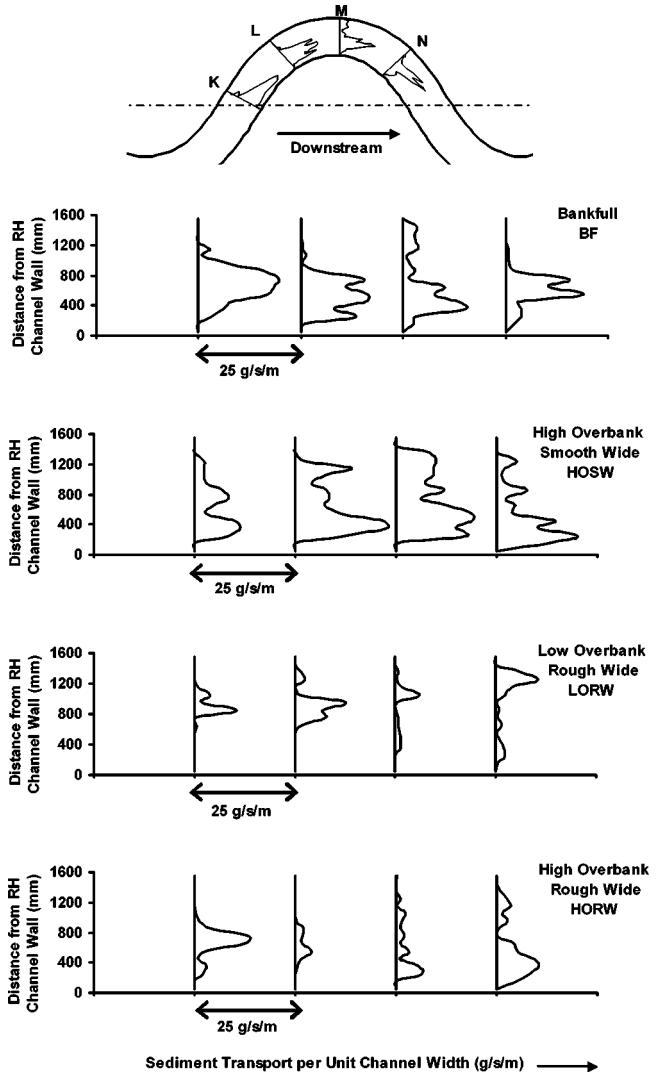

Fig. 17. Lateral distributions of bed load measured by the model Helley–Smith sampler

loads. This may be due to the fact that movement of bed forms would have a relatively greater effect on these low levels of sediment transport. It might also be that the Helley–Smith sampler is less accurate at these lower levels, since accurate positioning of the apparatus would be more critical.

Measurement of bed load using a sampler such as the Helley–Smith is known to be fraught with difficulties and sources of error, and these are likely to be exaggerated with the $\frac{1}{4}$-scale sampler. Even with this small sampler, it was still relatively large compared to the flow depth at some sampling locations, which would have adversely affected sampling efficiencies. In view of this, the comparisons between the integrated sampler readings and the total sediment measurements are surprisingly good. These results, whilst not necessarily accurate enough to provide a reliable integrated bed load rate at any cross-section, are sufficiently accurate to give a good estimate of the lateral distribution of bed load transport across the section.

The lateral distributions of bed load are shown in Fig. 17. It is apparent that bed load transport is not uniformly distributed laterally and, in many cases, it is noticeably concentrated within a narrow band.

In order to gain some insight into the mechanisms operating, values of bed load have been calculated for 100-mm-wide vertical increments across the channel using van Rijn's (1984a) bed load formula, modified for graded sediment and given as

$$Q_b = \sum_{i=1}^{i=n} 0.053 \cdot [(s-1)g]^{0.4} \cdot \nu^{0.2} \cdot d_i^{1.2} \cdot T^{2.1} \cdot p_i \cdot b \qquad (1)$$

where

$$T = \left(\frac{\tau - \tau_{\mathrm{cr}.i}}{\tau_{\mathrm{cr}.i}} \right) \qquad (2)$$

In this equation Q_b is the bed load (m^3/s) in each increment and is the sum of the bed load in n sediment size ranges (subscripted $i=1$ to n), with geometric mean diameters of d_i. τ is the bed shear stress, $\tau_{\mathrm{cr}.i}$ is the critical Shields bed shear stress for particles of diameter d_i, p_i is the proportion of particles of diameter d_i in the sediment, b is the lateral width of each increment (=100 mm). s is the relative density of the bed material, and ν is the kinematic viscosity of the water.

The authors investigated the possibility of determining the bed shear stress, τ, from the velocity readings using the log law of the wall. It was, however, found to be extremely unreliable. This is in part due to the fact that the log law is essentially a two-dimensional rigid bed theory and the assumptions upon which it is based do not necessarily apply in a highly three-dimensional mobile bed situation. In particular, the linear relationship $l=\kappa y$, where l is mixing length, y is distance from the wall, and κ is the Prandtl coefficient, which is assumed in the development of the log law, only strictly applies in the bottom 15–20% of relatively simple flows. It cannot be relied upon even to that extent in the highly three-dimensional flows observed in these experiments. Usable velocity readings would therefore need to be very close to the bed, and it is difficult to obtain accurate readings in this region with the acoustic Doppler velicometer (ADV) used in these experiments. Moreover, the log law of the wall requires an accurate determination of a notional bed level, which acts as a datum for vertical distance measurements. This is difficult to define in a mobile bed, and failure to correctly do so can lead to relatively large errors in the bed shear stress.

For the above-mentioned reasons the bed shear stress in each increment was evaluated using

$$\tau = \rho g \left[\frac{\overline{u}}{18 \log\left(\frac{12R}{3d_{90}} \right)} \right]^2 \qquad (3)$$

R=hydraulic radius of the lateral increment, which is assumed to be its mean depth and $\overline{u}$ is the observed depth averaged velocity in the increment. This is based upon the same logarithmic distribution discussed above, and is therefore subject to the same criticisms and reservations. However, it makes use of the depth averaged velocity, $\overline{u}$, and not simply those near to the boundary, which were difficult to measure accurately. It also does not rely so critically upon a correct determination of the notional bed level.

Eqs. (1) and (3) both assume a channel that is wide and straight, neither of which conditions applies in this case. However comparisons between the observed and calculated bed load distributions may be useful, since differences will reflect the effects due to meandering. Fig. 18 shows the comparisons between the observed and calculated lateral distributions of bed load. In order to facilitate comparison of the lateral distributions, the bed load is normalized as a ratio between the local bed load per unit width of flow (g/s/m) and the relevant mean value for the cross-section.

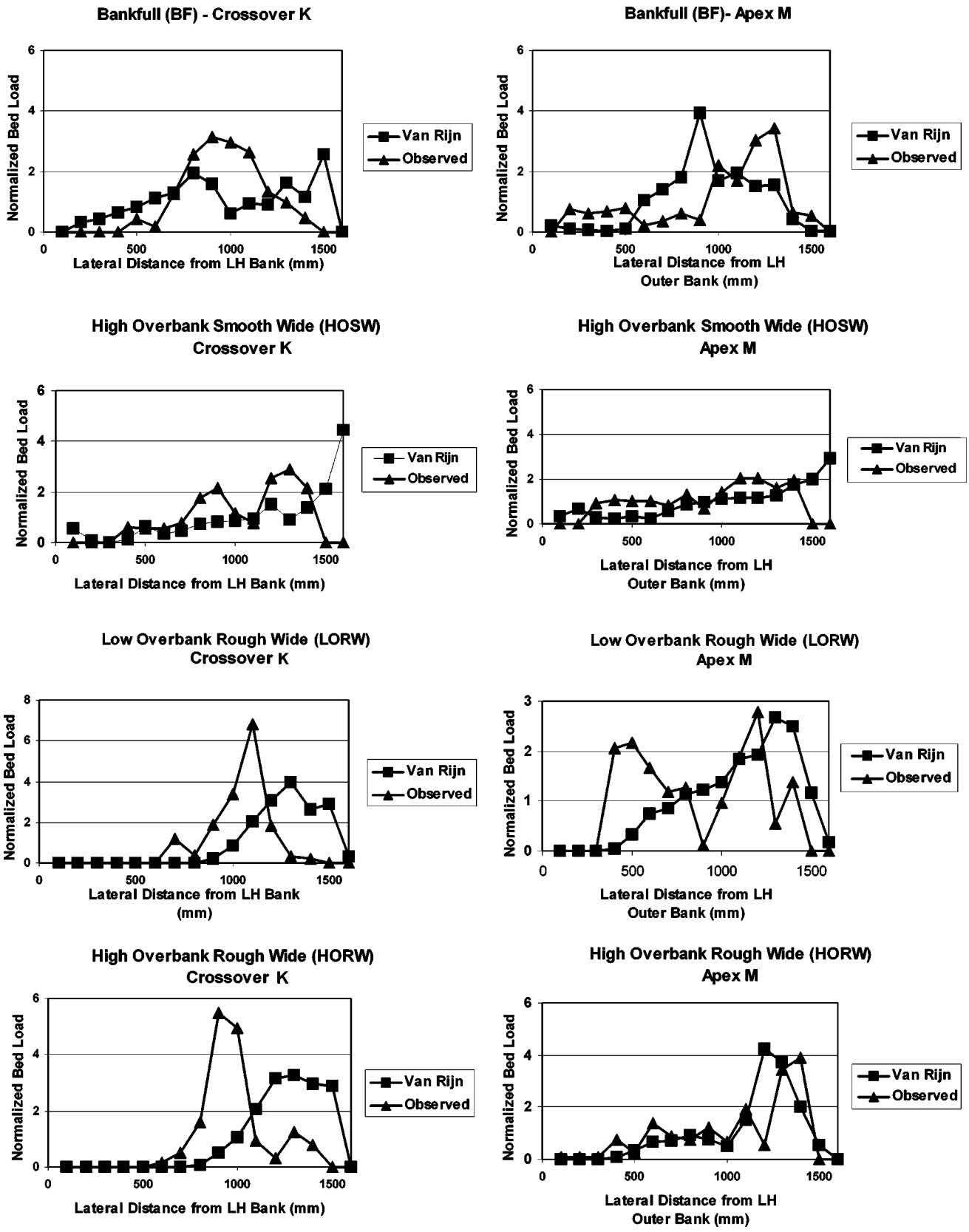

Fig. 18. Comparison of calculated and observed lateral bed load distributions. The bed load distributions are normalized to their mean values across each section.

For the bankfull (BF) case, Fig. 17 shows that the maximum sediment transport thread follows a path which tracks around the inside of the meander bend over the point bar and then crosses the channel to the inside of the next bend. It follows the shortest route through the meander. In Fig. 18 it is notable that the maximum observed bed load is nearer to the inside bank of the apex than its peak calculated value. This is due to the centrifugal circulation in this region, which is directed radially inwards at bed level and hence impels bed material in that direction.

For the high overbank smooth floodplain case (HOSW), the total sediment transport is considerably greater than at bankfull and somewhat more dispersed laterally. However the bulk of the material still moves around the inside of the bend. Just downstream of the apex the bed load becomes more concentrated near the inside bank of the bend. This is because the centrifugal circulation is strongly reinforced by the floodplain flows at this point which causes a strong secondary circulation with near-bed flows toward the inside of the bend. It is seen from Fig. 18 that the peak of the observed bed load is further away from the inside of the apex than the peak calculated bed load. This again reflects the secondary circulation at the apex, since the strong circulation generated at the upstream crossover, *K*, is carried through the apex.

The high overbank rough (HORW) bed load is much smaller than in the other two cases, although it still predominantly occurs over a limited part of the section. Fig. 18 shows that at the apex the maximum observed bed load is nearer the inner bank than the peak calculated value. This is similar to the bankfull case, although the lateral difference in peak values is less pronounced. This is to be expected, since the relatively weak interaction circulation from the upstream crossover, K, is insufficient to totally counteract the centrifugal circulation at the apex. However it does reduce it from its value at bankfull. At the crossover section, K, both overbank flows show an upstream shift of the peak observed bed load from its calculated value, which is due to the circulation cell generated by interaction between the main cannel and the floodplain. The bed load is shifted toward the inner bank just downstream of the apex for similar reasons to the smooth floodplain flow described above.

Comparison of Observed Sediment Transport with Bed Material Load Formulas

The observed sediment transport rate was compared with the values of bed material load calculated from two well-known transport formulas, namely, Ackers and White (1973), and van Rijn (1984a,b). The latter equation was applied in a modified form given by Pender and Li (1995). These two equations, as with all of the commonly used bed material formulas, essentially assume in their original derivation, (1) a homogeneous sediment and (2) a one-dimensional flow situation, i.e., no lateral flow variation. In these experiments a graded bed material was used. Moreover, the flow is highly three-dimensional with significant lateral variations in depth and velocity, and relatively large secondary circulation. Indeed the effect of this in shifting the lateral distribution of bed load has been demonstrated in the previous section. In view of this, considerable variation between observed and calculated bed material transport rates was expected. The purpose of this comparison was to obtain some initial pointers as to whether, and in what form, the bed material transport equations could be usefully employed in meandering channels. Thus the equations were applied at both crossover and apex sections, and the effect of allowing for sediment grading and/or lateral variation in flow and depth

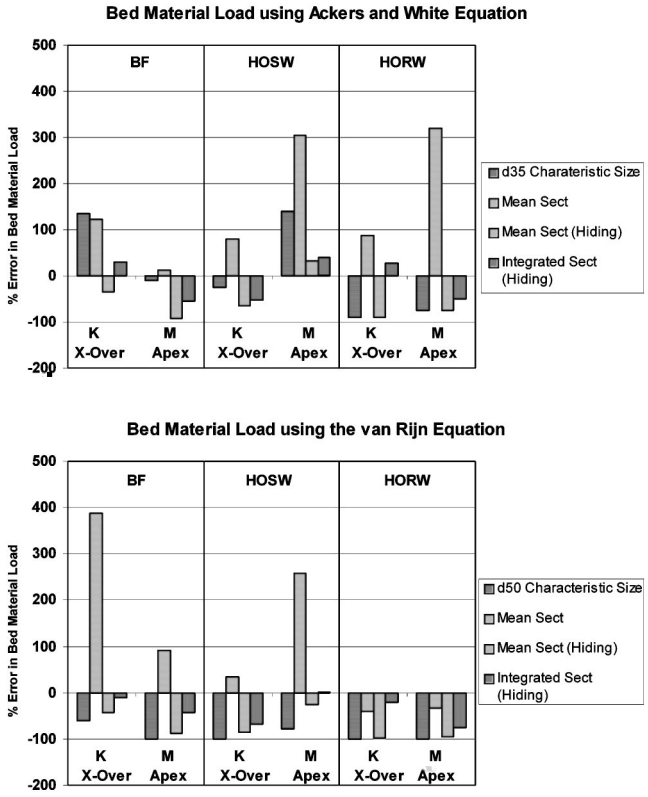

Fig. 19. Comparisons between calculated and observed bed material load values

were considered. The comparisons between observed and calculated bed material loads are shown in Fig. 19.

The Ackers/White equation is based upon the stream power concept described by Bagnold (1966). There are two van Rijn equations, one for bed load and one for suspended load. They are partially derived from physical considerations—first of the forces acting on saltating particles and, second, of suspended sediment concentration profiles. Although the derivations of the Ackers/White and van Rijn equations are quite different, they both make use, either directly or indirectly, of parameter T in Eq. (1). This represents the excess of actual bed shear stress over the Shields' critical value. Since the boundary shear stress is difficult to determine very accurately, and the parameter T depends on the difference between this and the critical Shields' value, which may be very similar in magnitude, both equations are particularly sensitive to errors in parameter T.

Both equations were originally derived for a homogeneous sediment represented by a characteristic grain size, which was taken as d_{35} for Ackers/White and d_{50} for van Rijn. Consequently the two equations were first applied, using their respective characteristic grain sizes, to the complete cross-sections using the mean depth, hydraulic radius, and velocity. The percentage errors in these results compared with the observed total sediment load (=100× {calculated total load—observed total load}/observed total load) are shown in Fig. 19 as d_{35} or d_{50} characteristic size.

In order to take account of the grading of the bed material, the equations were then applied to individual size fractions, which were summed to give the total bed material load in a similar fashion to Eq. (1). These results are shown in Fig. 19 as mean section.

In a mixture of grain sizes, there is a tendency for the smaller

Table 2. Mean Absolute Percentage Errors in Bed Material Load

Method	Ackers and White	Van Rijn
Characteristic size	79.7	89.7
Mean section	154.4	140.9
Mean section (hiding)	64.5	72.7
Integrated section (hiding)	42.2	37.3

grains to be hidden by the larger ones and hence to move less readily than in a homogeneous bed material. The larger grains, on the other hand, are more exposed than in a homogeneous material and tend to move more readily. This behavior of mixed grain sizes can be accommodated in the bed material load equations by use of hiding functions. Day (1980) and White and Day (1982) proposed a hiding function to be applied to the Ackers/White equation, which in effect adjusted the critical bed shear stress from its Shields' value for each size fraction. Proffitt and Sutherland (1983) extended this to a wider range of transport rates for each grain size, applying the hiding factor adjustment to the mobility function, F_{gr}, in the Ackers/White equation. Pender and Li (1995) investigated two hiding functions for the van Rijn equations. One was based upon the work of White and Day (1982) and the second upon the equal mobility concept of Parker (1991). Parker argued that initially the critical bed shear stress for all particles in a non-uniform sediment depends upon its geometric mean grain size. Thus this hiding function relates critical bed shear stress for each size fraction to the Shields' value for the overall material geometric mean size, rather than the Shields' value for the size fraction itself (as in the case for White and Day). Pender and Li found that this hiding function performed marginally better than that of White and Day and so it was adopted for the van Rijn equation in this investigation. These results are shown in Fig. 19 as mean section (hiding).

The calculations for the above-described bed load transport make use of average channel cross-section values as represented by mean depth, hydraulic radius, and velocity. However, the observed data showed considerable lateral variation of both depth and velocity in most cross-sections. In order to account for this the cross-section was divided into 100-mm-wide vertical strips and the load calculated for each strip using the observed depth of flow and depth mean velocity values. These results are shown in Fig. 19 as the integrated section (hiding).

It is clear from Fig. 19 that there are considerable differences between the calculated and observed values of bed material transport. As discussed above, this is to be expected bearing in mind the limiting assumptions made in the derivation of the equations and the complexity of the flow in meandering overbank channels. Nevertheless the results do provide pointers toward the application of these equations to meandering rivers.

The use of a single characteristic grain size gives relatively large errors. It is noticeable that in a number of instances the van Rijn equation gives no bed load transport (−100% difference), suggesting that a smaller characteristic size than the d_{50} may be more appropriate in this case. Modifying the equations to allow for sediment grading (mean section) gives calculated results which in many cases considerably overestimate the bed material load. This is due mainly to the excess transport of smaller grain sizes. Clearly some account must be taken of hiding in the non-uniform sediment. For both the Ackers/White and van Rijn formulas, the use of hiding functions considerably reduces the percentage error but generally leads to an underestimation of the bed material load. A further reduction in the errors is achieved by allowing for lateral variations in depth and velocity using the integrated section method. A rudimentary measure of this improvement is the mean absolute percentage error for the cross-sections shown in Fig. 19. These are shown in Table 2.

Clearly the integrated section method generally gives the most accurate values for bed material transport. However the errors are still considerable, and this must be due in part to the fact that secondary flows are not accounted for. It is noticeable that the error at the crossover section for bankfull flow is less than at the apex, where centrifugal circulation is greatest. In the smooth floodplain overbank case (HOSW), the error is largest at the crossover, where secondary circulation due to interaction with the high velocity floodplain flow is intense. At the apex where the interaction and centrifugal circulation cells virtually cancel each other, the error in bed material transport is less. In the rough overbank case (HORW) the interaction circulation at the crossover is not as large as in the smooth case, and neither is the error in bed material transport. However at the apex, where centrifugal circulation is established, the error in bed material transport is larger. Finally the results show that there are systematic differences between the van Rijn and Ackers/White equations. Whereas the former tends generally to underestimate the bed material transport, the latter overestimates it at those sections where the secondary circulation is relatively weak and *vice versa*.

A further source of error in the above application of the bed material transport equations is the assumption that the grain sizes in the exposed bed reflect the grading in the well-mixed parent material. The experiments were run first to equilibrium at bankfull and subsequently to equilibrium at overbank. Sorting of bed material occurred which reflected this flow history. The variation in exposed grain sizes can be seen in the aerial photographs of the bed, Figs. 6 and 10. Clearly there is considerable variation in the grading of the exposed bed material both longitudinally and laterally.

Summary and Conclusions

- A series of experiments have been carried out, on the U.K. Flood Channel Facility (FCF) at HR Wallingford, to investigate the effect of bankfull and overbank flows on the bed morphology of a meandering channel in a floodplain.
- The flow structure in meandering channels with overbank flow is essentially determined by two processes (1) centrifugal circulation generated around the meander bend and (2) circulation due to main channel/floodplain interaction in the region of the crossover section. The circulation generated by interaction has opposite polarity to the centrifugal circulation at the next downstream bend. The relative strengths of these opposing circulation cells determine the structure of the flow, in particular around the bend.
- All experimental runs were performed by first allowing the main channel to reach equilibrium conditions at bankfull flow, thus allowing the formation of a bed profile to match that in real rivers. This bed profile exhibited the classic riffle-pool sequence at crossover and bend apex, respectively, and also a point bar at the inside of the bend.
- The influence of overbank flow on the morphology of the bend depended upon the roughness of the floodplain, which determined the intensity of the interaction circulation generated around the crossover. This counteracted the centrifugal circulation around the bend, which in the case of both smooth and rough floodplains led to erosion of the inner point bar. However, in the case of the smooth floodplain the interaction cir-

culation was strong enough through the bend to cause deposition around the outside bank. With the rough floodplain, the net circulation around the bend was not strong enough either to maintain the point bar or cause deposition around the outside of the bend. This led to increased net erosion of bed material around the apex which was deposited downstream to form an enhanced point bar.

- The overall sediment transport rate was seen to fall as the flow went overbank and to reach a minimum at a depth ratio in the region of 0.15–0.25. This reinforces the notion of bankfull as being the dominant channel forming flow.
- Lateral distribution of bed load was measured using a $\frac{1}{4}$-scale Helley–Smith sampler. Although there was variation between the cross-sections, the average bed load integrated from these readings around a meander agreed surprisingly well with measurements of total sediment load. The lateral bed load distribution in most cases displayed a distinct peak. At bankfull, this peak bed load took the shortest route through the meanders, with centrifugal circulation shifting it toward the inside bank around each bend. With overbank flow, the path of the peak bed load was modified in accordance with the secondary circulation. In particular it was shifted strongly toward the inside bank just downstream of the apex where centrifugal circulation is strongly reinforced by floodplain flows.
- The Ackers/White and van Rijn bed material load equations were compared with the observed sediment load for bankfull and overbank flows at crossover and bend sections. The comparisons showed that significantly improved results could be obtained by modifying the equations to handle individual sediment size fractions, using hiding functions and by integrating them across the section, using observed local depth and velocity values. However the errors in the equations were still large. One source of error is that secondary flows are ignored and a perceived link between the size of the error and the magnitude of the secondary circulation suggests that this might be the case. Another source of error is that the exposed bed material is variable and does not have the same grading as the parent sediment. It is clear that the bed material transport equations do not give reliable results in these complex flow situations; indeed they were not designed to do so. Their effective use in such situations may be restricted to within the context of a properly designed two- or three-dimensional numerical model.
- Overbank flow with meandering main channels is a complex, but commonly occurring, condition in real rivers. It is becoming increasingly widespread with the greater use of two-stage channels as flood channels. There is relatively little previous work reported on this, and much of that has been limited to rigid bed channels. It is demonstrated how overbank flows can considerably modify a river's bed morphology, and this in turn feeds back to alter flow structures. More work is required to unravel in detail the complex reactions of a meandering main channel to overbank flows. In particular the time frame of these adjustments with relation to flood hydrographs. Nevertheless it is clearly demonstrated that significant adjustments in main channel morphology and flow structure undoubtedly occur, and these may well need to be incorporated into reliable numerical models for the prediction of discharge and sediment transport in rivers.

Acknowledgments

The authors wish to acknowledge the financial support of the U.K. EPSRC and the help and advice of members of staff at Hydraulics Research Wallingford United Kingdom throughout this work.

Notation

The following symbols are used in this paper:

b = incremental lateral width;
d = particle diameter;
p = proportion of graded particles on a size range;
Q_b = bed load (m^3/s) in lateral increment width b;
R = hydraulic radius;
s = relative density of bed material;
$T=(\tau-\tau_{cr}/\tau_{cr})$ = dimensionless shear parameter;
$\overline{u}$ = depth mean velocity;
ν = kinematic viscosity;
τ = bed shear stress; and
τ_{cr} = critical bed shear stress.

References

Ackers, P., and White, W. R. (1973). "Sediment transport: New approach and analysis." *J. Hydraul. Div., Am. Soc. Civ. Eng.*, 99(11), 2041–2060.

Bagnold, R. A. (1966). "An approach to general sediment transport problem from general physics." *U.S. Geological Survey Professional Paper No. 422-J*.

Day, T. J. (1980). "A study of the transport of graded sediments." *Rep. No. IT 190*, Hydraulic Research, Wallingford, U.K.

Dietrich, W. E. (1987). "Mechanics of flow and sediment transport in river bends." *River Channels—Environment and Process*, K. Richards, ed., Basil Blackwell, Oxford, U.K., 129–227.

Dietrich, W. E., and Smith, J. D. (1984)~11980

Hydraul. Res., 28(4), 417–436.
Parker, G., and Andrews, E. D. (1985). "Sorting of bedload sediments by flow in meander bends." *Water Resour. Res.*, 21, 1361–1373.
Pender, G., and Li, Q. (1995). "Comparison of two hiding function formulations for non-uniform sediment transport calculations." *Proc. Inst. Civ. Eng., Waters. Maritime Energ.*, 112, 127–135.
Proffitt, G., and Sutherland, A. J. (1983). "Transport of non-uniform sediments." *J. Hydraul. Res.*, 21(1), 33–43.
Rameshwaran, P., Spooner, J., Shiono, K., and Chandler, J. H. (1999). "Flow mechanisms in two-stage meandering channel with mobile bed." *Proc., XXVIII Congress of the Int. Assoc. of Hydraulic Research*, Graz, Austria (CD-ROM).
Sellin, R. H. J., Bryant, T., and Loveless, J. H. (2003). "An improved method for roughening floodplains on physical river models." *J. Hydraul. Res.*, 41(1), 3–14.
Sellin, R. H. J., Ervine, D. A., and Willetts, B. B. (1993). "Behaviour of meandering two-stage channels." *Proc. Inst. Civ. Eng., Waters. Maritime Energ.*, 101, 99–111.
Shiono, K., and Muto, Y. (1998). "Complex flow mechanisms in compound meandering channels with overbank flow." *J. Fluid Mech.*, 376, 221–261.
van Rijn, L. C. (1984a). "Sediment transport part I: bed load transport." *J. Hydraul. Eng.*, 110(10), 1431–1456.
van Rijn, L. C. (1984b). "Sediment transport. III: Bed forms and alluvial roughness." *J. Hydraul. Eng.*, 110(12), 1733–1754.
White, R. W., and Day, T. J. (1982). "Transport of graded gravel bed material." *Gravel Bed Rivers*, R. D. Hey, et al., ed., Wiley, New York, 181–213.
Wolman, M. G., and Miller, J. P. (1960). "Magnitude and frequency of forces in geomorphic processes." *J. Geol.*, 68, 54–74.
Wormleaton, P. R., Sellin, R. H. J., Bryant, T., Loveless, J. H., Hey, R. D., and Catmur, S. E. (2004). "Flow structures in a two-stage channel with a mobile bed." *J. Hydraul. Res.*, 42(2), 145–162.